

REVIEW OF RIGOROUS COUPLED-WAVE ANALYSIS AND OF  
HOMOGENEOUS EFFECTIVE MEDIUM APPROXIMATIONS FOR  
HIGH SPATIAL-FREQUENCY SURFACE-RELIEF GRATINGS

by

*Elias N. Glytsis, David L. Brundrett, and Thomas K. Gaylord*  
*School of Electrical Engineering and Microelectronics Research Center*  
*Georgia Institute of Technology, Atlanta, Georgia 30332*  
*Tel. No. (404) 894-8415 / (404) 894-2931*

ABSTRACT

A review of the rigorous coupled-wave analysis as applied to the diffraction of electromagnetic waves by gratings is presented. The analysis is valid for any polarization, angle of incidence, and conical diffraction. Cascaded and/or multiplexed gratings as well as material anisotropy can be incorporated under the same formalism. Small period rectangular groove gratings can also be modeled using approximately equivalent uniaxial homogeneous layers (effective media). The ordinary and extraordinary refractive indices of these layers depend on the grating filling factor, the refractive indices of the substrate and superstrate, and the ratio of the freespace wavelength to grating period. Comparisons of the homogeneous effective medium approximations with the rigorous coupled-wave analysis are presented. Antireflection designs (single-layer or multilayer) using the effective medium models are presented and compared. These ultra-short period antireflection gratings can also be used to produce soft x-rays. Comparisons of the rigorous coupled-wave analysis with experimental results on soft x-ray generation by gratings are also included.

I. INTRODUCTION

The diffraction of electromagnetic waves by periodic structures continues to be of great practical importance owing to numerous applications in a variety of fields such as acousto-optics, integrated optics, spectroscopy, optical interconnects, binary optics, and quantum electronics. Furthermore, high spatial-frequency (small period compared to wavelength) surface-relief binary or multilevel staircase diffraction gratings on dielectric or lossy substrates can behave as homogeneous uniaxial layer(s) for either polarization and angle of incidence. As a result these gratings can be used in applications such as in high-power lasers, antireflection surfaces, filters similar to thin-film coatings, wave plates, and polarization-selective mirrors.

In this paper a brief review of the rigorous coupled-wave analysis is presented along with the effective medium approximations for high spatial-frequency gratings. The analysis

is valid for any incident polarization and angle of incidence. The orientation of the plane of incidence can also be arbitrary (conical diffraction). The electric and magnetic fields in the grating region can be expanded in terms of spatial harmonics which must satisfy Maxwell's equations. The resulting set of first-order coupled differential equations can be solved simultaneously with the boundary conditions of the problem leading to the determination of all quantities of interest (diffracted fields, efficiencies). The review of the rigorous coupled-wave analysis is presented in sec. II.

In the small period limit, all diffracted orders except the zeroth orders are cutoff and the grating behaves like a slab of homogeneous uniaxial material (effective medium) with its optic axis parallel to the grating vector. The ordinary and the principal extraordinary indices of the slab depend on the grating filling factor (duty cycle), the refractive indices of the substrate and the surrounding medium, and the ratio of the freespace wavelength to period. These refractive indices can be determined by solving two transcendental equations (higher-order refractive indices). Approximate solutions of the transcendental equations define the second-order indices (second-order dependence on wavelength-to-period ratio), and first-order indices (no dependence on the wavelength-to-period ratio). The diffraction efficiencies using the effective medium models are compared with those obtained by the rigorous coupled-wave analysis for various diffraction geometries. The wavelength-to-period ratio necessary for the validity of each model is determined. The effective medium approximations are presented in sec. III.

Antireflection behavior can be obtained by appropriate combinations of the filling factor and the groove depth of the grating. Design procedures are presented using the higher-order, the second-order, and the first-order grating refractive indices and are compared. Multilevel stairstep gratings are also designed to perform like broadband antireflection filters (Butterworth or Chebyshev). The design of antireflection gratings is described in sec. IV.

Finally, small period gratings can be used in conjunction with intense femtosecond laser pulses to produce sub-picosecond soft x-rays through the creation of a plasma grating. Antireflection grating design is needed to minimize the reflectance of these grating targets. The rigorous coupled-wave analysis was applied to analyze photolithographically produced SiO, Si, and SiN gratings with subwavelength periods. These results are presented in sec. V.

## II. RIGOROUS COUPLED-WAVE ANALYSIS

Methods of grating diffraction analysis can be divided into two major categories, the integral methods,<sup>1</sup> and the differential methods.<sup>1-7</sup> The most common and accurate differential methods are coupled-wave approaches<sup>2-5</sup> and modal approaches.<sup>6,7</sup>

The general geometry of a grating structure along with an incident plane wave is shown in Fig. 1. This figure corresponds to a surface-relief type grating but it applies

to volume gratings too. The grating and the surrounding regions can be general anisotropic. The configuration in Fig. 1 corresponds to any general three-dimensional incidence and any allowable linear polarization. The electric and magnetic fields in the grating region(s) are expanded in terms of spatial harmonics  $\vec{E} = \sum_i \vec{S}_i(z) \exp(-j\vec{\sigma}_i \cdot \vec{r})$  and  $\vec{H} = (\epsilon_0/\mu_0)^{1/2} \sum_i \vec{U}_i(z) \exp(-j\vec{\sigma}_i \cdot \vec{r})$ , where  $\vec{\sigma}_i = \vec{k}_{inc} - i\vec{K}$  ( $i = 0, \pm 1, \pm 2, \dots$ ),  $\vec{S}_i, \vec{U}_i$  are the space harmonic amplitudes,  $\vec{k}_{inc}$  is the incident wavevector (in the grating region),  $\vec{K}$  is the grating vector, and  $\epsilon_0, \mu_0$  are the permittivity and permeability of freespace, and  $\omega$  is the angular frequency of the incident wave. The field expansions must satisfy Maxwell's curl equations in the grating region(s):

$$\begin{aligned}\vec{\nabla} \times \vec{E} &= -j\omega \vec{B} = j\omega\mu_0 \tilde{\mu}(x, z) \vec{H}, \\ \vec{\nabla} \times \vec{H} &= \vec{J} + j\omega \vec{D} = [j\omega\epsilon_0 \tilde{\epsilon}(x, z) + \tilde{\sigma}(x, z)] \vec{E},\end{aligned}\tag{1}$$

where  $\tilde{\epsilon}, \tilde{\mu}$ , and  $\tilde{\sigma}$  are the relative permittivity, relative permeability, and conductivity tensors of the grating regions and are periodic in the direction of the grating vector. More general equations can be written if constitutive relations of the form  $\vec{D} = \tilde{\epsilon} \vec{E} + \tilde{g} \vec{H}$  and  $\vec{B} = \tilde{h} \vec{E} + \tilde{\mu} \vec{H}$  (for bianisotropic media) are used where  $\tilde{g}$  and  $\tilde{h}$  are the coupling tensors between  $\vec{D}$  and  $\vec{H}$ , and  $\vec{B}$  and  $\vec{E}$ . However, the most common and practical case in optics is when only the permittivity tensor is modulated. Using the spatial expansions of the fields into Eq. (1) an infinite set of linear coupled-wave differential equations is derived. If the infinite number of possible diffracted orders is truncated to a finite number  $m$  then the total number of coupled-wave equations becomes  $6m$ . Eliminating the components along the propagation direction ( $z$  in Fig. 1), the tangential components of the electric and magnetic fields can be expressed in the following compact matrix form<sup>3-5</sup>

$$d\tilde{V}/dz = j\tilde{A}\tilde{V},\tag{2}$$

where  $\tilde{V}$  is a  $4m \times 1$  vector containing the tangential space harmonic components of the electric and magnetic fields and  $\tilde{A}$  is a  $4m \times 4m$  coupling matrix.<sup>3-5</sup> All special cases can be derived from the above general expression. For example if angle  $\alpha = 0^\circ$  (Fig. 1) and  $\psi = 90^\circ$ , only the  $y$ -components of the electric field and the  $x$ -components of the magnetic field exist (TE polarization) and Eq. (2) reduces to a system of  $2m$  equations. Similarly, Eq. (2) reduces to  $2m$  equations in the case of  $\alpha = 0^\circ$  and  $\psi = 0^\circ$  (TM polarization). The above conclusions in these limiting cases are valid if isotropic or special orientation (with respect to the principal axes) anisotropic grating region(s) are considered. In general, for three-dimensional incidence (conical diffraction) the two orthogonal polarizations are coupled even in the isotropic case. Independently of the grating characteristics Eq. (2) can be solved in the form  $\tilde{V} = \tilde{W} \exp(\tilde{\Lambda}z) \tilde{C}$ , where  $\tilde{W}$  and  $\tilde{\Lambda}$  contain the eigenvectors and eigenvalues of the coupling matrix  $\tilde{A}$ , and  $\tilde{C}$  contains  $4m$  unknown constants.<sup>2-4</sup> Combining the previous field solutions with the known plane wave solutions in the regions external to the grating, a set of boundary conditions is formed. Solution of this set of conditions (a linear system of the form  $Ax = b$ ) specifies all the unknown field coefficients.<sup>3-5</sup> Knowledge of the electric

and magnetic fields in any region of the problem determines all quantities of interest, such as the diffraction efficiencies. The same approach is valid for any type of volume or surface-relief grating of constant or varying modulation since they can be represented as cascaded gratings.<sup>5</sup> The same formulation can be applied to multiplexed gratings.<sup>5</sup> The effective medium approximations for a high spatial-frequency surface-relief grating are presented in the next section.

### III. HOMOGENEOUS EFFECTIVE MEDIUM APPROXIMATIONS

A high spatial-frequency surface-relief grating is characterized by a period  $\Lambda$  which is much smaller than the incident freespace wavelength  $\lambda_0$ . In this case all the diffracted orders except the zero forward-diffracted and the zero backward-diffracted orders are cutoff. This is shown schematically in Fig. 2a for a rectangular-groove grating in the case of conical diffraction geometry. A cross section of the grating is shown in Fig. 2b. The superstrate and substrate refractive indices are  $n_1$  and  $n_3$  respectively, while the filling factor of the grating is  $F$ . The grating vector is  $\vec{K} = \hat{x}(2\pi/\Lambda)$  where  $\hat{x}$  is the unit vector along the  $x$  direction.

In the case that  $\lambda_0 \gg \Lambda$  it can be shown<sup>8,9</sup> that at normal incidence for TE polarization (electric field polarized perpendicular to the grating vector,  $\vec{E} \perp \vec{K}$ ) there is an effective refractive index  $n_O$  defined, which is given by

$$n_O = [n_1^2(1-F) + n_3^2 F]^{1/2}. \quad (3)$$

For the orthogonal polarization (TM polarization or magnetic field perpendicular to the grating vector,  $\vec{H} \perp \vec{K}$ ), the corresponding effective refractive index  $n_E$  is given by

$$n_E = \left[ \frac{1-F}{n_1^2} + \frac{F}{n_3^2} \right]^{-1/2}. \quad (4)$$

In the general case of oblique incidence the high spatial-frequency grating is equivalent<sup>10,11</sup> to a uniaxial homogeneous slab with its optic axis oriented along the direction of the grating vector ( $x$  direction in this case), and ordinary and extraordinary refractive indices given by Eqs. (3) and (4) respectively or by the higher-order indices defined next. The thickness of the slab is equal to the groove depth  $d$  of the grating. The effective indices given by Eqs. (3) and (4) are the first-order indices and they are denoted by  $(n_O^{(1)}, n_E^{(1)})$  in contrast to the second- and higher-order effective indices which are presented next.

Higher-order approximations of the effective ordinary and extraordinary indices have been found by Rytov.<sup>12</sup> These indices are given by the solutions of the following transcendental equations:

$$\begin{aligned} \sqrt{n_1^2 - n_O^2} \tan \left[ \frac{\Lambda}{\lambda_0} \pi (1-F) \sqrt{n_1^2 - n_O^2} \right] &= - \sqrt{n_3^2 - n_O^2} \tan \left[ \frac{\Lambda}{\lambda_0} \pi F \sqrt{n_3^2 - n_O^2} \right], \\ \frac{\sqrt{n_1^2 - n_E^2}}{n_1^2} \tan \left[ \frac{\Lambda}{\lambda_0} \pi (1-F) \sqrt{n_1^2 - n_E^2} \right] &= - \frac{\sqrt{n_3^2 - n_E^2}}{n_3^2} \tan \left[ \frac{\Lambda}{\lambda_0} \pi F \sqrt{n_3^2 - n_E^2} \right]. \end{aligned} \quad (5)$$

The effective refractive indices which are solutions of the above equations are denoted as higher-order effective indices  $(n_O^{(H)}, n_E^{(H)})$ . Approximate solutions of Eqs. (5) with second-order dependence on the grating period to wavelength ratio, are characterized as second-order effective indices  $(n_O^{(2)}, n_E^{(2)})$  and are given by

$$\begin{aligned} n_O^{(2)} &= [(n_O^{(1)})^2 + \frac{1}{3}[\pi \frac{\Lambda}{\lambda_0} F(1-F)]^2 (n_3^2 - n_1^2)^2]^{1/2}, \\ n_E^{(2)} &= [(n_E^{(1)})^2 + \frac{1}{3}[\pi \frac{\Lambda}{\lambda_0} F(1-F)]^2 (\frac{1}{n_3^2} - \frac{1}{n_1^2})^2 (n_E^{(1)})^6 (n_O^{(1)})^2]^{1/2}. \end{aligned} \quad (6)$$

The higher- and second-order effective indices converge to the first-order indices when  $(\Lambda/\lambda_0) \rightarrow 0$ . The modeling of a high spatial-frequency surface-relief grating through a uniaxial homogeneous layer using the first-, second-, or higher-order effective indices constitutes the effective medium models that can approximate the grating behavior.

The dependence of the three different effective indices [Eqs. (3), (4), (5), and (6)] on the filling factor of the grating is shown in Fig. 3a for  $\lambda_0/\Lambda = 5$  and for a silicon grating at  $\lambda_0 = 1.5 \mu\text{m}$  in air ( $n_1 = 1$ ,  $n_3 = 3.5$ ). The dependence of the effective indices on  $\lambda_0/\Lambda$  is shown in Fig. 3b for  $F = 0.5$ . It is apparent that the three effective indices pairs differ substantially, especially for small  $\lambda_0/\Lambda$  ratios. For large ratios ( $\lambda_0/\Lambda > 15$ ) the higher- and the second-order indices are essentially the same as the first-order effective indices.

The same uniaxial homogeneous slab model with ordinary and extraordinary indices given by the first-, second-, or higher-order effective indices can also be used in the more general case of the conical diffraction as long as all diffracted orders except the zero forward-diffracted (transmitted) order and the zero backward-diffracted (reflected) order are cutoff. To demonstrate the validity of the models for the conical diffraction case, a silicon grating of  $F = 0.22$  and  $d = 0.134\lambda_0$  is used at  $\lambda_0 = 1.5 \mu\text{m}$  for a polar and azimuthal angles of incidence (Fig. 2)  $\theta = \phi = 45 \text{ deg}$  and TE polarization. The zero-order backward-diffracted efficiency is shown in Fig. 4 using each of the three approximate models (using the first-, second- and higher-order effective indices) and using the rigorous coupled-wave analysis. It is observed that the second- and the higher-order models agree very well with the exact solution obtained with the rigorous coupled-wave analysis even for small  $\lambda_0/\Lambda$  ratios ( $\approx 2$ ). Consequently, these effective medium models can be used for the design of surface-relief gratings even with larger periods compared to the incident freespace wavelength. These models will be exploited next in order to design antireflection gratings on silicon substrates.

#### IV. ANTIREFLECTION GRATING DESIGNS

As was shown previously, high spatial-frequency gratings can be well approximated by homogeneous uniaxial layers with effective ordinary and extraordinary refractive indices which depend on the grating parameters, the incident wavelength and the refractive indices of the surrounding media. Thus, results from the thin layer designs can be used for the design of antireflection gratings. Antireflection grating designs on dielectrics, semiconductors

or metals, similar to thin film antireflection coatings designs, are well documented in the literature.<sup>8,9,13-16</sup>

The antireflection grating design procedure is analogous to the microwave wave-impedance matching technique. For a single layer antireflection coating (equivalent to a single-level rectangular groove grating) its thickness and refractive index are given by

$$d = \frac{\lambda_0}{4N_2} p, \quad N_2 = \sqrt{N_1 N_3}, \quad (7)$$

where  $p = 1, 3, 5, \dots$ , and  $N_1, N_2, N_3$  are the effective indices that correspond to the wave impedance in the superstrate, the effective uniaxial layer, and the substrate. The  $N_2$  is a function of the first-order, second-order, or higher-order refractive indices of the homogeneous uniaxial layer. Equations (7) can be solved either analytically (in the case that first-order effective indices are used) or numerically (in the case that second- or higher-order refractive indices are used) with respect to  $F$  and  $d$ . The solutions using the second- or the higher-order effective indices depend on the  $\lambda_0/\Lambda$  ratio. These designs can be greatly improved over the first-order designs which do not depend on  $\lambda_0/\Lambda$  ratio. Example antireflection designs of single-level rectangular-groove gratings are shown in Figs. 5. Specifically, the filling factor and the groove depth needed to suppress completely (according to the homogeneous layer approximation) the specular reflection are shown in Figs. 5a-b, and 5c as a function of the polar angle of incidence  $\theta$  for four distinct cases of incident light of  $\lambda_0 = 1.5 \mu\text{m}$  on silicon targets in air ( $\phi = 0$  or  $90$  deg and for TE or TM incident polarization).

The same principles can be generalized to design broadband antireflection gratings similar to broadband antireflection thin film coatings<sup>16</sup>. These designs resemble the microwave Butterworth or Chebyshev transformers. The resulting grating is a multilevel stairstep grating as shown in Fig. 6. The detailed procedure is summarized in Ref. 16. An example design on silicon at  $\lambda_0 = 1.5 \mu\text{m}$  is shown in Table I for a two- and a three-level maximally-flat (Butterworth) and equal-ripple (Chebyshev) filters using the first-order effective indices at normal incidence. The resulting reflectivity of these gratings is shown in Figs. 7a and 7b where the broadband antireflection response is apparent.

Antireflection grating designs can be obtained even for gratings with small  $\lambda_0/\Lambda$  ratio. In these cases the approximate effective medium models will not approximate the grating accurately. However, the designs obtained by the effective medium models can again be of significant value since they can serve as starting designs which can be improved by using the rigorous coupled-wave analysis and a simulated annealing type of algorithm.

## V. ANTIREFLECTION GRATINGS FOR X-RAY EMISSION

Laser produced plasmas created by intense femtosecond laser pulses have been demonstrated to produce subpicosecond soft-x-rays.<sup>17,18</sup> The use of terawatt femtosecond lasers

permits the generation of more intense x-ray sources. However, increased target reflectivity at high fluence results in less efficient coupling. Grating targets can dramatically increase this coupling.<sup>8</sup> The rigorous coupled-wave analysis was applied to analyze photolithographically produced SiO, Si, and SiN diffraction surface-relief gratings with varying groove depths and filling factors and with periods of 240 or 300 nm. Good agreement between the experimental data and the calculated rigorous coupled-wave results was obtained (Figs. 8a and 8b). The plasma gratings are inhomogeneous due to the varying plasma temperature. However, the rigorous coupled-wave analysis can be applied since the plasma grating can be decomposed into a series of cascade homogeneous gratings. Specially designed antireflection gratings could potentially increase absorption resulting in an enhanced energy deposition, a hotter plasma, and consequently more intense x-ray emission.

## VI. SUMMARY

A review of the rigorous coupled-wave analysis of grating diffraction was presented. The analysis is valid for both volume or surface-relief gratings and can incorporate lossy or anisotropic materials. The same formalism is also applicable to cascaded and/or multiplexed gratings. In addition, a review of the effective medium approximations as applied to small period surface-relief gratings was also presented. It was shown that high spatial-frequency gratings can be modeled as uniaxial homogeneous layers with their optic axis parallel to the grating vector. The ordinary and extraordinary indices of the layers depend on the grating parameters and the ratio of the grating period to the freespace wavelength. Three effective medium models were defined using first-, second-, and higher-order indices. It was demonstrated that the effective medium models are also valid in the case of conical diffraction. Applications of the first-order model to single-level and multilevel antireflection gratings were presented. Experimental comparisons of the rigorous coupled-wave analysis results on soft x-ray generating gratings were also included.

## VII. REFERENCES

- [1] R. Petit, Ed., *Electromagnetic Theory of Gratings*, Springer-Verlag, 62 (1980).
- [2] H. Kogelnik, *Bell Syst. Tech. J.* **48**, 2909 (1969).
- [3] M. G. Moharam and T. K. Gaylord, *J. Opt. Soc. Am.* **71**, 811 (1981).
- [4] T. K. Gaylord and M. G. Moharam, *Proc. IEEE* **73**, 894 (1985).
- [5] E. N. Glytsis and T. K. Gaylord, *J. Opt. Soc. Am. A* **7**, 1399 (1990).
- [6] T. Tamir, H. C. Wang, and A. A. Oliner, *IEEE Trans. Microwave Theory Tech.* **MTT-12**, 323 (1964).
- [7] R. S. Chu and J. A. Kong, *IEEE Trans. Microwave Theory Tech.* **MTT-25**, 18 (1977).
- [8] Y. Ono, Y. Kimura, Y. Ohta, and N. Nishida, *Appl. Opt.* **26**, 1142 (1987).
- [9] T. K. Gaylord, W. E. Baird, and M. G. Moharam, *Appl. Opt.* **25**, 4562 (1986).
- [10] R. C. McPhedran, L. C. Botten, M. S. Craig, M. Neviere, and D. Maystre, *Opt. Acta*

- 29, 289 (1982).
- [11] G. Bouchitte and R. Petit, *Electromag.* **5**, 17 (1985).
  - [12] S. M. Rytov, *Soviet Phys. JETP-2*, 466 (1956).
  - [13] T. K. Gaylord, E. N. Glytsis, and M. G. Moharam, *Appl. Opt.* **26**, 3123 (1987).
  - [14] E. N. Glytsis and T. K. Gaylord, *Appl. Opt.* **27**, 4288 (1988).
  - [15] T. K. Gaylord, E. N. Glytsis, M. G. Moharam, and W. E. Baird, *U. S. Patent No. 5,007,708* (1991).
  - [16] E. N. Glytsis and T. K. Gaylord, *Appl. Opt.* **31**, 4459 (1992).
  - [17] M. Murnane, H. Kapteyn, J. Bokor, W. Mansfield, R. Gnall, E. N. Glytsis, T. K. Gaylord, and R. Falcone, *OSA Topical Meeting on Short Wavelength Coherent Radiation*, Monterey, CA, April 1991.
  - [18] M. Murnane, H. Kapteyn, J. Bokor, W. Mansfield, E. N. Glytsis, and R. Falcone, *Appl. Phys. Lett.*, 1993 (accepted).

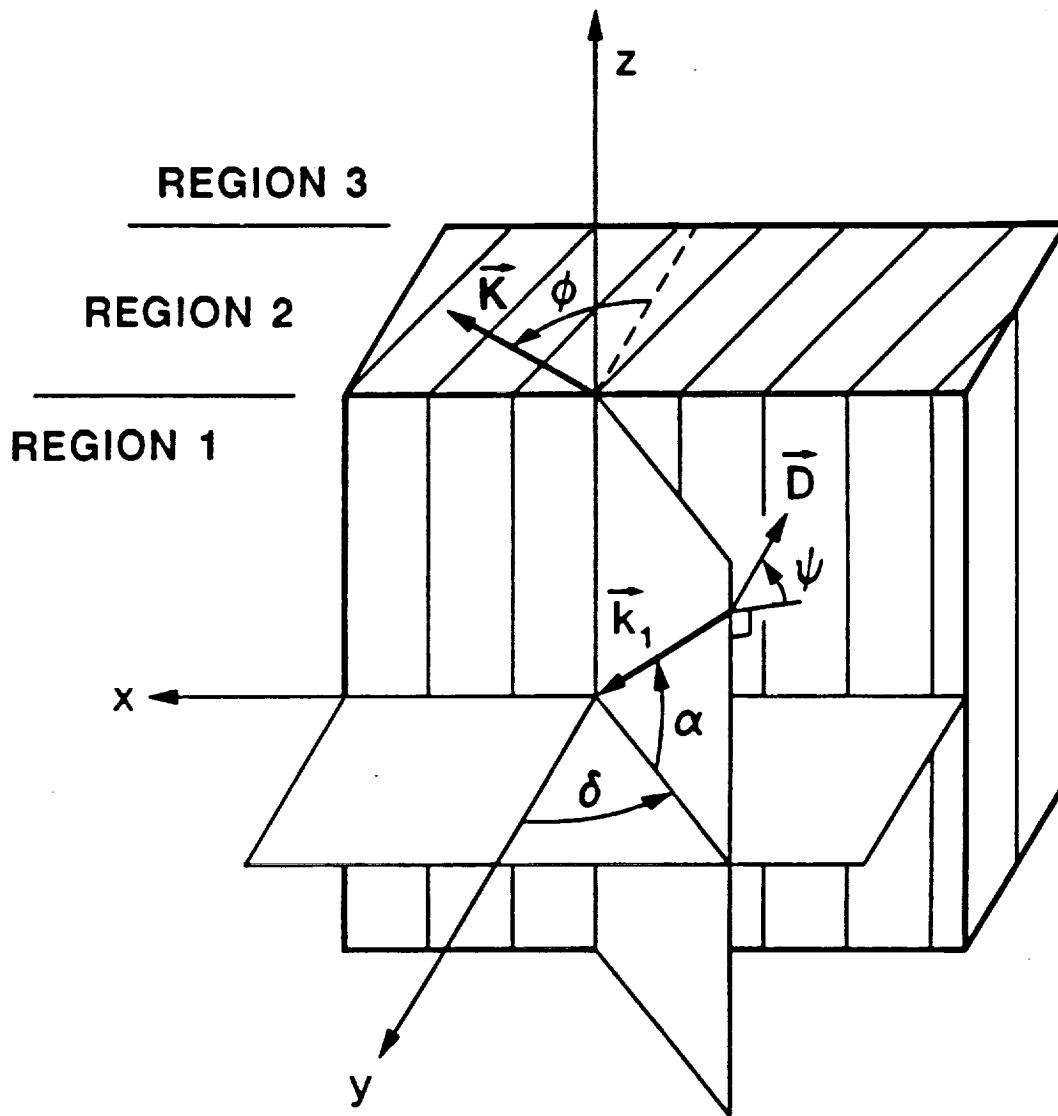


**Fig. 1:** The three-dimensional geometry of the grating structure and the incident plane wave. The angle of incidence is  $\gamma$  (in the plane of incidence). The angles  $\alpha$  and  $\delta$  are used to specify the incident wavevector in the  $xyz$  coordinates system. The angle  $\psi$  specifies the angular orientation of the incident polarization. An angle  $\alpha = 0$  deg and  $\psi = 90$  deg corresponds to TE polarization while an angle  $\alpha = 0$  deg and  $\psi = 0$  deg corresponds to TM polarization.

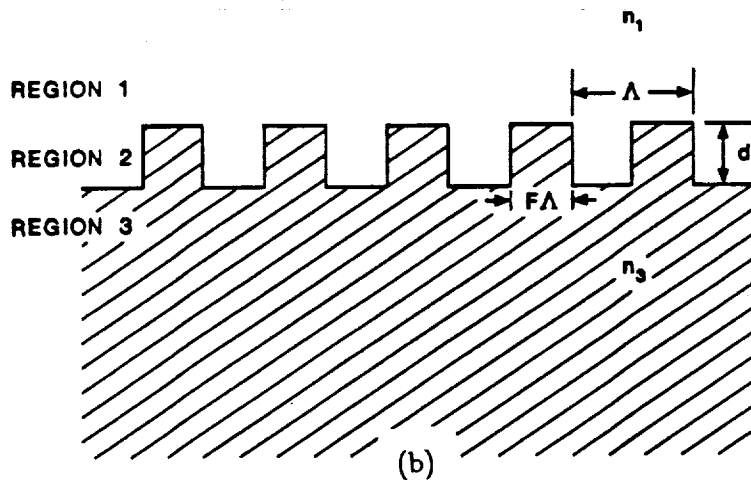
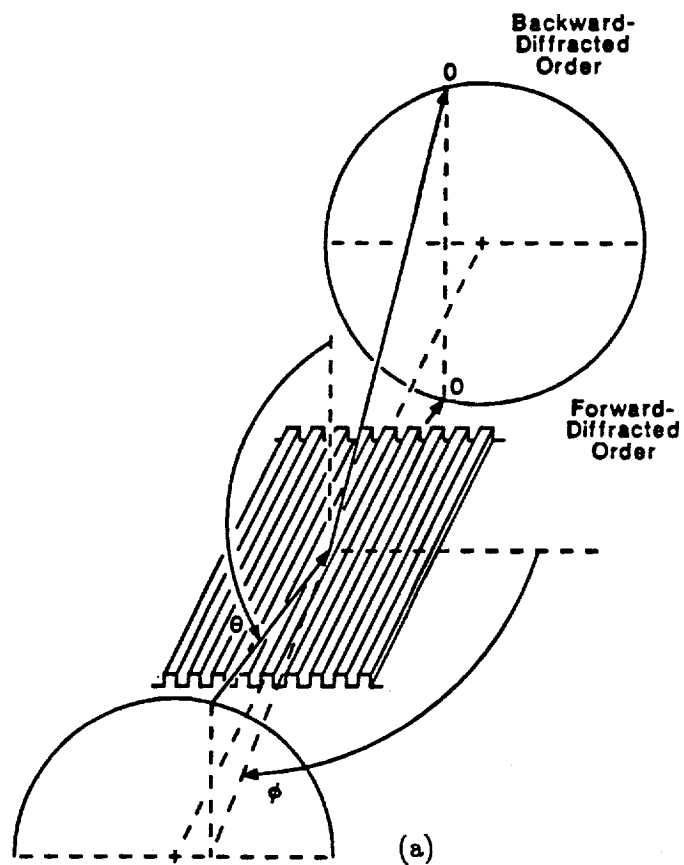


**Fig. 2:** (a) A high spatial-frequency rectangular groove surface-relief grating in the case of conical diffraction. Only the zero backward- and zero forward-diffracted orders are propagating as shown by their corresponding wavevectors. (b) A cross-sectional view of the rectangular groove high spatial-frequency grating.

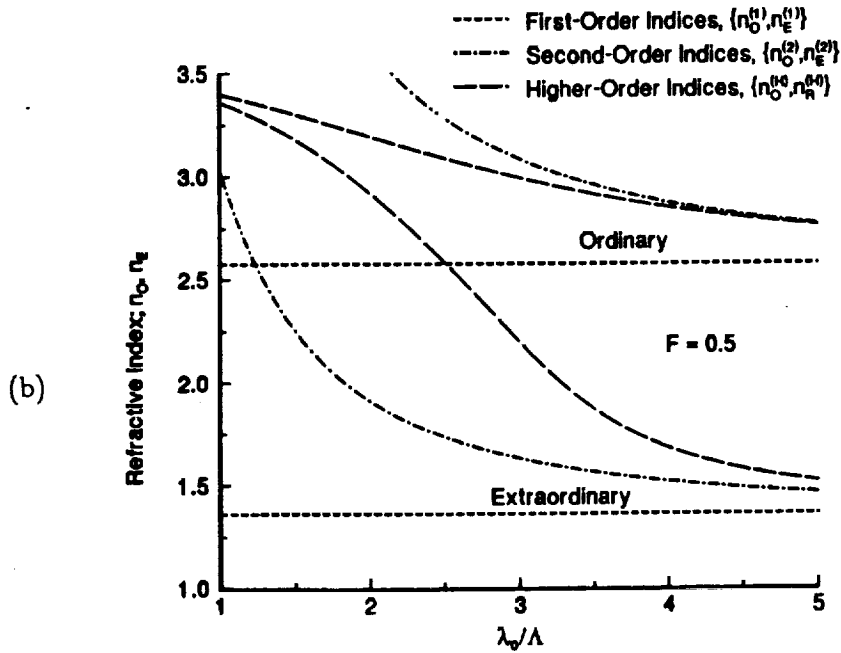
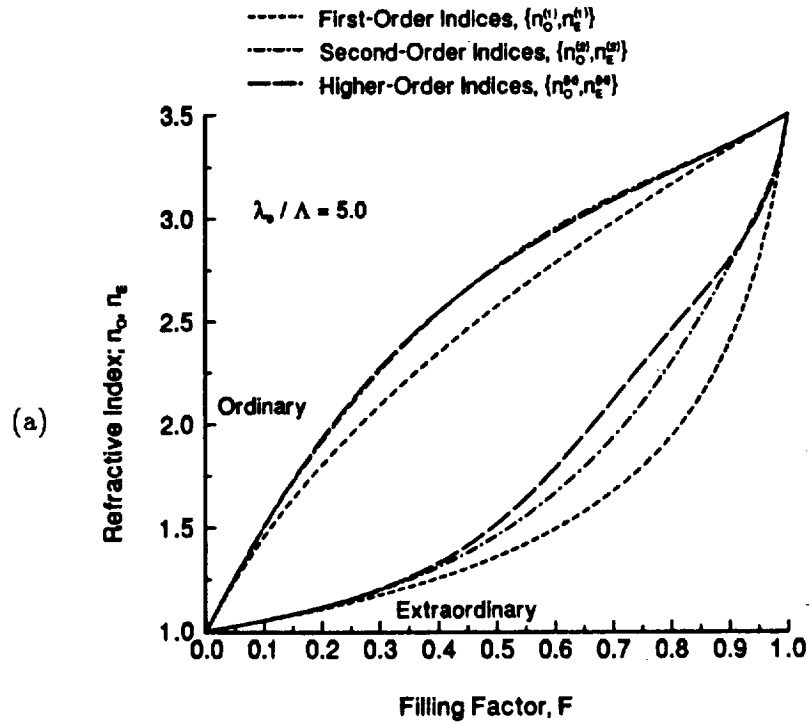


**Fig. 3:** (a) Dependence of the first-, second- and higher-order effective refractive indices (ordinary and extraordinary) on the filling factor of a rectangular groove grating for  $\lambda_0/\Lambda = 3$ . (b) Dependence of the first-, second- and higher-order effective refractive indices (ordinary and extraordinary) on the  $\lambda_0/\Lambda$  of a rectangular groove grating with  $F = 0.5$ .

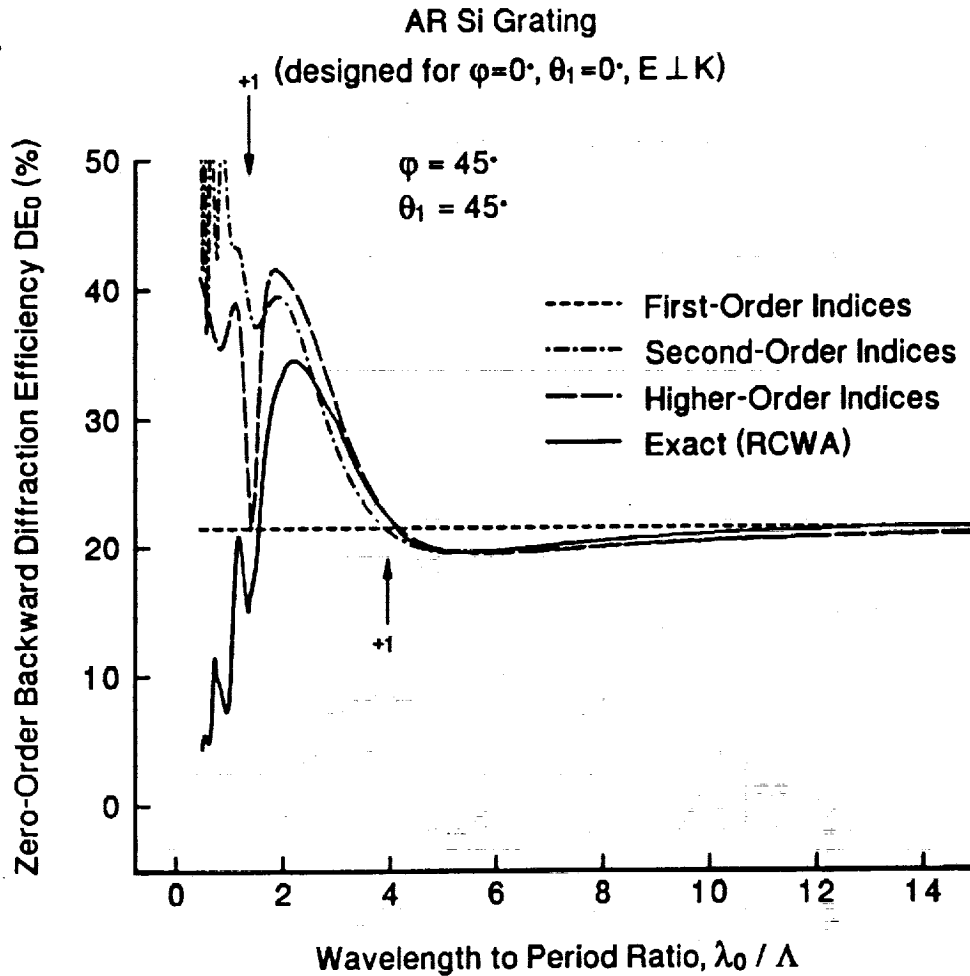


**Fig. 4:** The zero-order backward-diffracted efficiency of a silicon grating for  $\lambda_0 = 1.5 \mu\text{m}$  in the conical diffraction case ( $\phi = \theta = 45 \text{ deg}$ ) as a function of  $\lambda_0 / \Lambda$ . The results using the approximate models (with first-, second-, and higher-order indices) as well as the exact results using the rigorous coupled-wave analysis are shown.

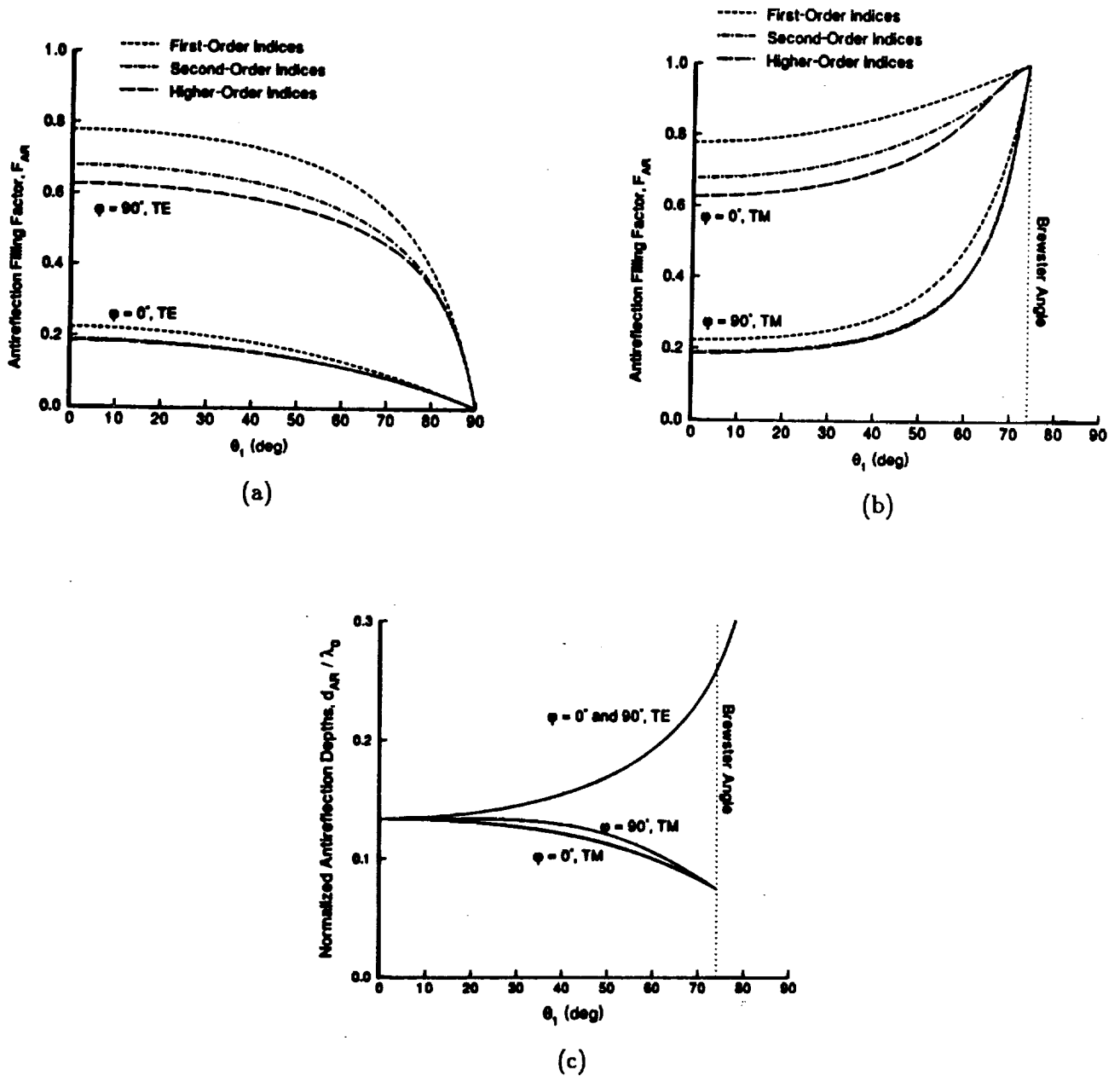


**Fig. 5:** The filling factor  $F$  of a rectangular groove surface-relief antireflection grating on silicon substrate at  $\lambda_0 = 1.5 \mu\text{m}$  and at  $\lambda_0/\Lambda = 3.0(?)$  as a function of the polar angle of incidence  $\theta$ : (a) for  $\phi = 0$  or  $90^\circ$  and TE incident polarization, and (b) for  $\phi = 0$  or  $90^\circ$  and TM incident polarization. (c) The corresponding normalized groove depths ( $/\lambda_0$ ) of the antireflection gratings for the same cases as in (a) and (b).

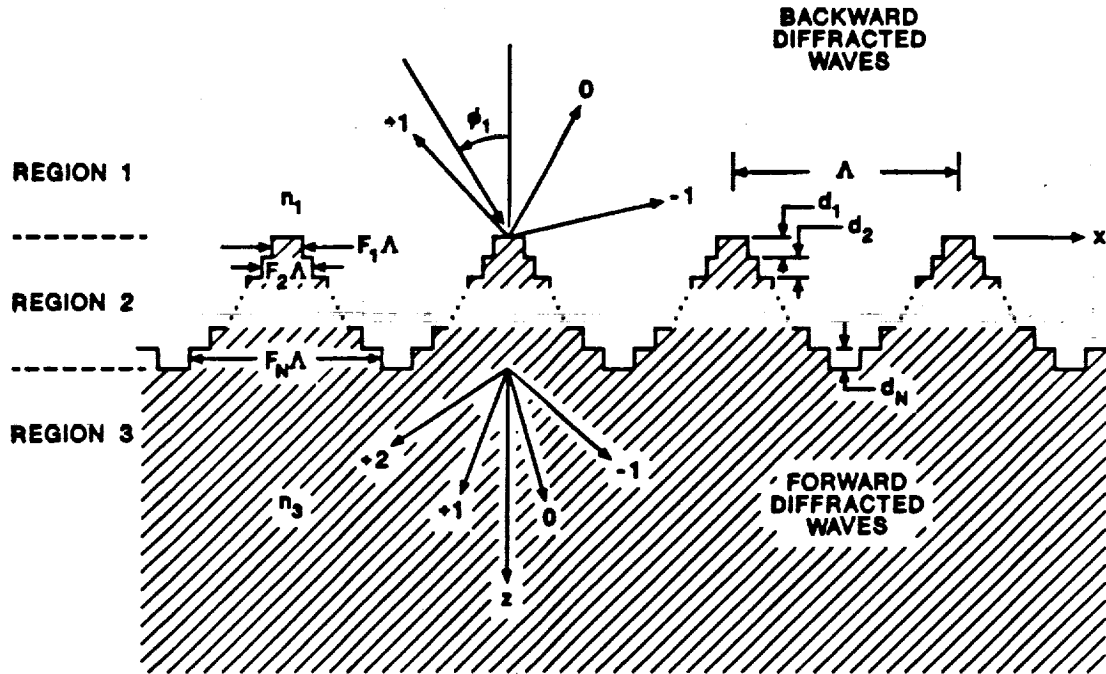
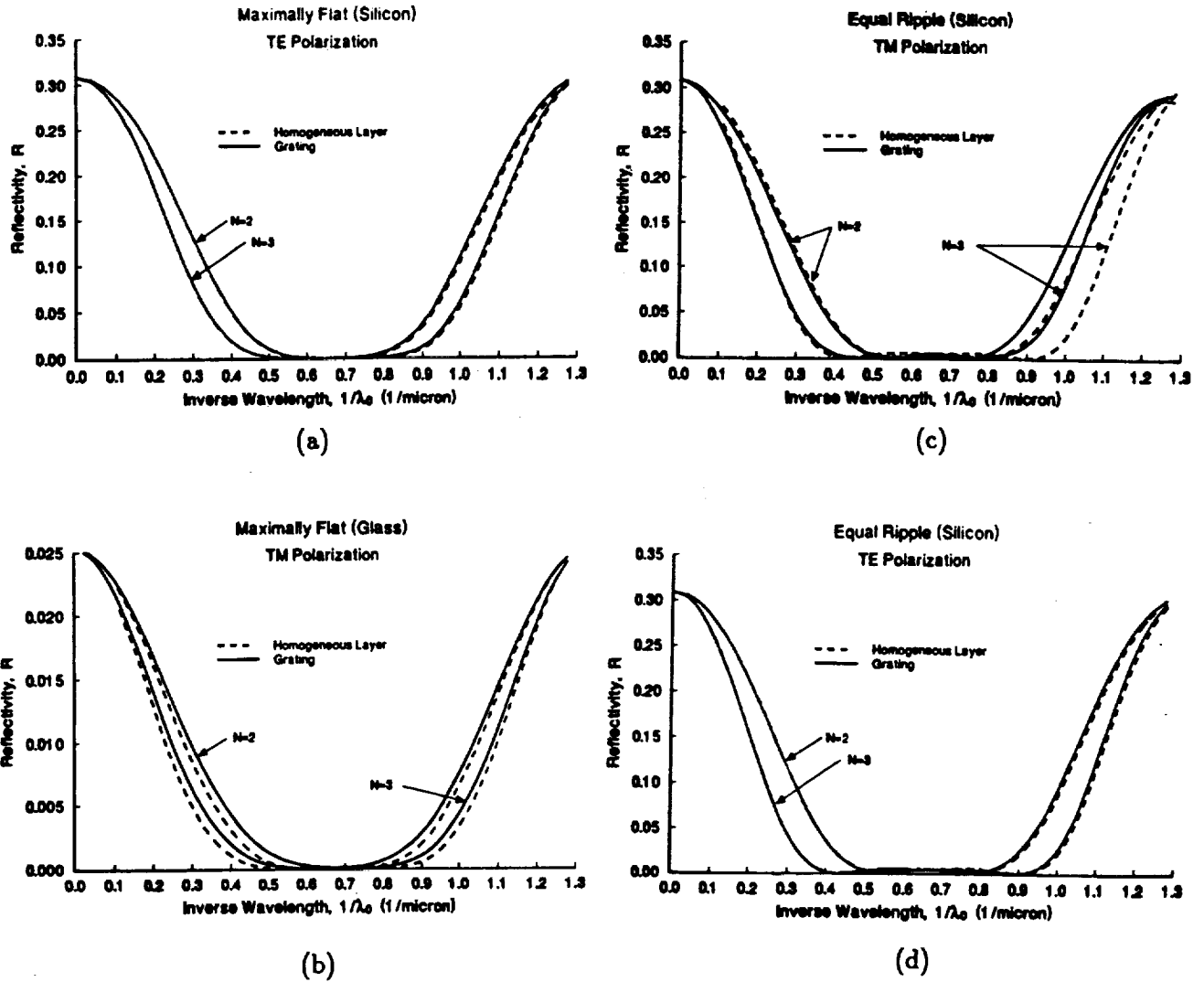


Fig. 6: Cross-sectional view of a multilevel ( $N$ -level) stairstep surface relief grating.

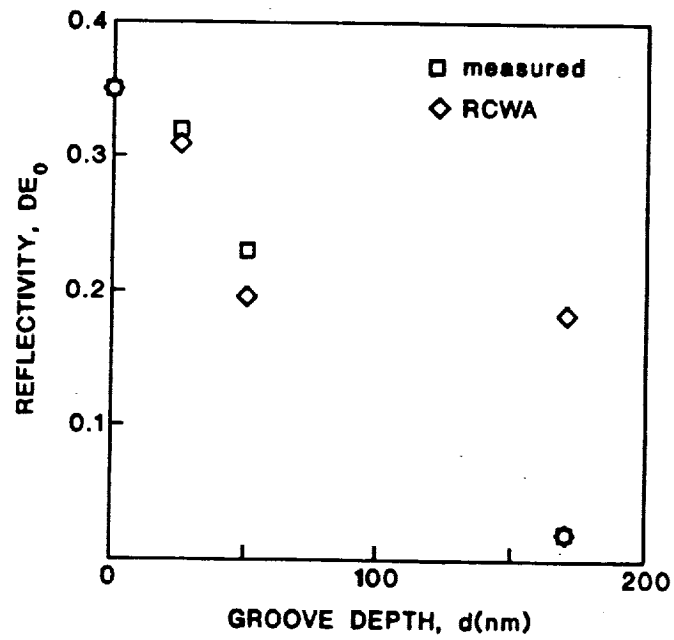
Table I: Grating Broadband Antireflection Surfaces on Silicon

Design parameters for grating quarter-wave (broadband antireflection surfaces) transformers for normal ( $\phi_1 = 0^\circ$ ) incidence on silicon ( $n_3 = 3.5$ ) at center freespace wavelength  $\lambda_0 = 1.5\mu\text{m}$ . The filling factors  $F_{TE}$  (for TE polarization),  $F_{TM}$  (for TM polarization) and the groove depths  $d_i$ 's, are summarized for two and three section maximally flat and equal-ripple transformers. Input region is air ( $n_1 = 1.0$ ).

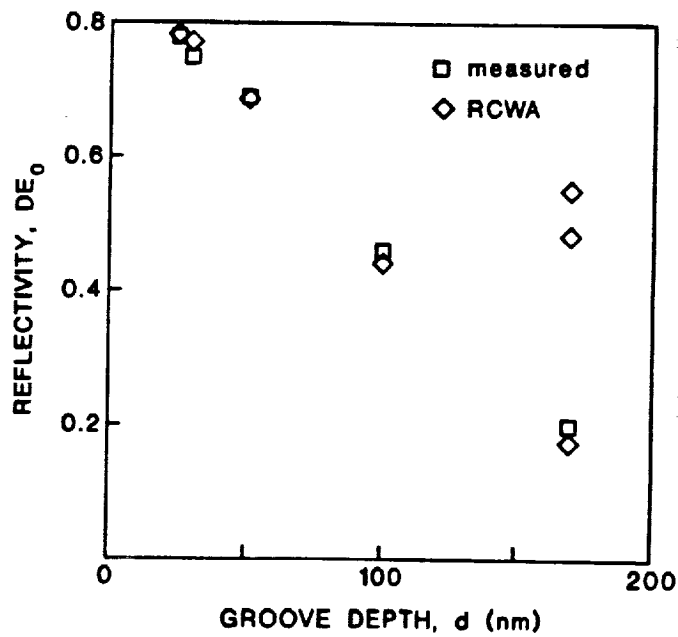
Levels	Layer	Maximally-Flat			Equal-Ripple		
		$d_i$ ( $\mu\text{m}$ )	$F_{TE}$	$F_{TM}$	$d_i$ ( $\mu\text{m}$ )	$F_{TE}$	$F_{TM}$
2	1	0.2742	0.0774	0.5068	0.2821	0.0682	0.4727
	2	0.1465	0.4931	0.9226	0.1612	0.3923	0.8877
3	1	0.3206	0.0327	0.2928	0.3202	0.0330	0.2951
	2	0.2004	0.2222	0.7778	0.2139	0.1842	0.7345
	3	0.1253	0.7072	0.9673	0.1429	0.5229	0.9307



**Fig. 7:** Reflectivity  $R$  (zero-order backward-diffracted efficiency) of a silicon multilevel surface-relief maximally-flat antireflection grating for 2 or 3 levels as a function of the inverse wavelength at normal incidence. The solid curves represent the rigorous coupled-wave analysis results while the dashed lines represent the effective homogeneous layer which first-order indices results; (a) for TE polarization and (b) for TM polarization. (c) and (d) the same results for an equal-ripple antireflection grating.



(a)



(b)

**Fig. 8:** Comparison of experimental and theoretical data (computed using the rigorous coupled-wave analysis) for different Si gratings using single or double cascaded gratings approximations. (a) Silicon gratings at room temperature, (b) silicon plasma gratings.